atmosphere

MDPI

Article

Atmospheric Particulate Selenium Deposition in Semi-Arid Croplands of the Chinese Loess Plateau: Enrichment, Fluxes, and Contributions to External Inputs

Xuezhen Li [1], Yiren Duan [2], Zhiliang Wu [3], Kun Lin [4,*], Tao Yu [5,6,*] and Zhongfang Yang [5,7,*]

1 Institute of Earth Sciences, China University of Geosciences, Beijing 100083, China
2 School of Earth Sciences and Engineering, Nanjing University, Nanjing 210093, China
3 Harbin Natural Resources Survey, China Geological Survey, Harbin 150086, China
4 College of Natural Resources and Environment, South China Agricultural University, Guangzhou 510642, China
5 Key Laboratory of Ecological Geochemistry, Ministry of Natural Resources, Beijing 100037, China
6 School of Science, China University of Geosciences, Beijing 100083, China
7 School of Earth Sciences and Resources, China University of Geosciences, Beijing 100083, China
* Correspondence: link1213@scau.edu.cn (K.L.); yutao@cugb.edu.cn (T.Y.); yangzf@cugb.edu.cn (Z.Y.)

Abstract

Irrigation is often regarded as a major external source of selenium (Se) to croplands, yet the contribution of atmospheric deposition remains insufficiently quantified in semi-arid agricultural regions, where limited and variable irrigation may increase its relative importance. In this study, we monitored atmospheric particulate Se deposition at 16 sites in western Yuanzhou on the Chinese Loess Plateau, and assessed its contribution to cropland Se inputs under different irrigation scenarios. Deposited particles contained 2.43–4.86 times the Se concentration of neighboring bulk topsoils (median concentration ratio: 3.59). Annual collector-derived particulate Se fluxes were 0.501–1.715 g ha^{-1} yr^{-1} (median: 0.710). The mean atmospheric inputs exceeded the estimated fertilizer inputs in all three major geomorphic units but were lower than irrigation inputs at the reference volume. At the reference irrigation volume of 2130 m^3 ha^{-1} yr^{-1} and standardized fertilizer rate of 750 kg ha^{-1} yr^{-1}, the median atmospheric contribution to the combined Se inputs from deposition, irrigation and fertilizer was 14.91% across the assessed dryland raster cells. Under locally informed supplemental irrigation references of 1200 and 750 m^3 ha^{-1} yr^{-1}, median contributions increased to 22.85% and 30.92%, respectively. The area where deposition supplied at least one quarter of quantified inputs expanded from 2503 ha (3.43%) to 26,344 ha (36.08%) and 55,288 ha (75.73%), respectively. These scenario-based estimates depend on prescribed irrigation and fertilizer inputs and do not represent measured field-specific contributions. The findings highlight the spatially variable importance of atmospheric Se deposition to semi-arid croplands and its sensitivity to irrigation water inputs.

Keywords: atmospheric particulate deposition; selenium; cropland selenium budget; irrigation sensitivity; semi-arid croplands

Check for updates

Academic Editor: Kei Sato

Received: 23 October 2026
Revised: 12 November 2026
Accepted: 16 November 2026
Published: 18 November 2026

Copyright: © 2026 by the authors. Licensee MDPI, Basel, Switzerland. This article is an open access article distributed under the terms and conditions of the Creative Commons Attribution (CC BY) license.

1. Introduction

Atmospheric deposition links the atmosphere with terrestrial ecosystems and supplies selenium (Se) to soils as part of its biogeochemical cycle [1–3]. Se released by natural processes and human activities reaches the land surface through atmospheric transport, gas–particle conversion, and deposition. Its chemical speciation and deposition fluxes are jointly

influenced by emission sources, meteorological conditions, and atmospheric chemistry. Global observations and modeling have characterized atmospheric Se emission and deposition patterns and identified uncertainties in source attribution and process parameters [4–6]. Regional observations further show that the composition of deposited Se and other trace elements varies with aerosol sources and weather dynamics [7,8]. On the Chinese Loess Plateau, dust transport and deposition are prominent processes; differences in dust sources, particle sorting, and mineral composition may influence trace-element distributions in particles [9,10]. The relative enrichment of Se in deposition particles does not, by itself, indicate the annual Se supply. Particle composition or large-scale deposition models alone cannot establish the amount of Se delivered to specific croplands. Regional measurements of deposition fluxes therefore need to be considered alongside particle geochemistry.

Se cycling in croplands involves inputs from atmospheric deposition, irrigation, and fertilization, and outputs through crop harvest, leaching, and volatilization [3,11–13]. Budget studies indicate that the relative importance of these pathways differs among agricultural regions. Yu et al. [13] quantified multiple Se input and output pathways in an agricultural area of Sichuan, China. Song et al. [14] estimated that atmospheric deposition accounted for 84.90% of quantified Se inputs in the Hamatong River Basin of the Sanjiang Plain. Chen et al. [15] reported respective contributions of 70.93%, 27.35%, and 1.72% from atmospheric deposition, irrigation, and fertilization across nine counties in central-eastern Guangxi. These regional differences show why deposition fluxes need to be assessed alongside other agricultural inputs. Irrigation water Se concentration and irrigation volume determine the estimated irrigation input and can alter the relative contribution of atmospheric deposition. Irrigation conditions may also affect Se speciation and mobility after it enters soil [16,17]. This issue is particularly relevant in semi-arid agricultural regions where precipitation is seasonally concentrated and dryland and irrigated croplands coexist. Irrigation scenarios grounded in regional management conditions can help assess how atmospheric contributions vary across plausible levels of water use. Comparing atmospheric input with crop harvest export does not account for other output processes [13,14]. Over longer timescales, topsoil Se stocks are also influenced by geological sources, soil formation, and other biogeochemical processes [3,18]. Atmospheric Se deposition should therefore be evaluated in relation to both annual cropland input pathways and existing soil Se stocks.

Western Yuanzhou District, Ningxia, lies in the semi-arid Chinese Loess Plateau. Mean annual precipitation is approximately 488.2 mm and occurs mainly in summer. Dryland croplands account for 84.3% of the effective agricultural area, and the major geomorphic units comprise valley plains, red-bed hills and loess hills. Previous studies have linked local soil Se distributions to geological sources, soil formation and hydrological transport [19,20]. We combined deposition monitoring, neighboring soil geochemistry and agricultural samples to (1) characterize the composition of Se and associated elements in deposition particles relative to neighboring topsoils and quantify annual particulate Se deposition and its spatial variation; (2) compare the Se inputs from atmospheric deposition, irrigation, and fertilization, and quantify atmospheric contribution shares and the areas exceeding specified contribution thresholds under a regional water volume reference scenario and locally informed supplemental irrigation scenarios; and (3) compare atmospheric Se input with estimated crop harvest Se export and reference estimates of other Se outputs, as well as Se stocks in the 0–20 cm topsoil, to assess the annual supply in relation to both agricultural outputs and the existing soil inventory.

2. Materials and Methods

2.1. Study Area

The study area is located in western Yuanzhou District, Guyuan City, Ningxia Hui Autonomous Region, China, within the semi-arid Loess Plateau. The climate is temperate continental monsoonal, with mean annual precipitation of approximately 488.2 mm, concentrated mainly from July to September. Valley plains, red-bed hills, and loess hills constitute the major geomorphic units, with spatial differences in soil parent materials and hydrological conditions [19,20]. Maize and potato are the principal crops, and agricultural land consists mainly of dryland and irrigated croplands. Within the effective agricultural area of western Yuanzhou, dryland and irrigated croplands cover 73,008.54 and 13,634.39 ha, respectively; dryland croplands account for 84.3%. Figure 1 shows the study area and sampling locations.

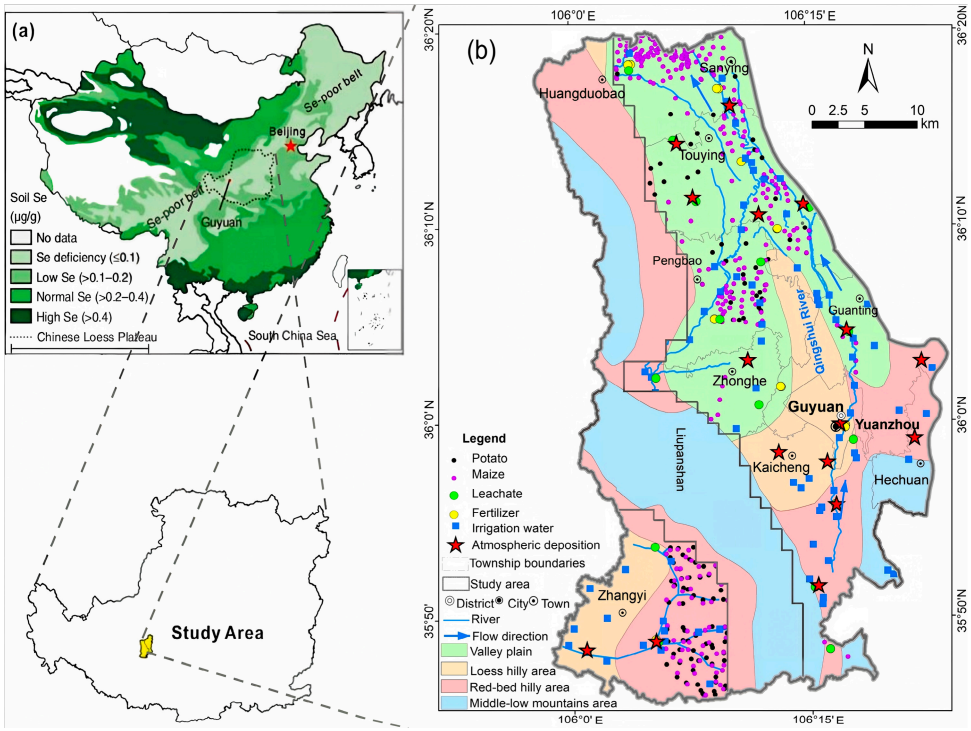


Figure 1. Study area and sampling locations: (**a**) national soil Se distribution adapted from Blazina et al. [21], with a regional location inset; (**b**) geomorphic units and sampling locations in western Yuanzhou, Ningxia, China. Red stars identify the 16 atmospheric deposition sites; separate symbols distinguish maize, potato, irrigation water, fertilizer and percolating water sampling locations. Coincident locations overlap: 55 fertilizer samples represent 14 distinct coordinate pairs, and 91 water samples represent 90. Mountain terrain is shown for geographic context. Blue arrows indicate river flow direction.

2.2. Sample Collection and Preparation

2.2.1. Atmospheric Deposition

From May 2019 to April 2020, atmospheric deposition was monitored at 16 sites across the geomorphic units of western Yuanzhou: seven in the valley plain, five in the red-bed hilly area, and four in the loess hilly area. High-density polyethylene collectors with an effective opening area of 0.036644 m^2 were used. Sites were located away from obvious local pollution sources and obstructions such as tall trees and buildings. Collectors were generally placed on flat roofs of village houses or other elevated locations and were recovered once after a full year of exposure.

Samples were allowed to settle after recovery. The supernatant was acidified with 5 mL HNO_3 diluted 1:1 (v/v) and filtered through a 0.45 µm polyester membrane. Particles were dried below 65 °C, weighed and analyzed for Se, Cd, Zn, Pb, Cr and Ni. Liquid-fraction Se was reported below 0.01 µg L^{-1}. The reported Se flux represents recovered particles; dissolved Se flux was not quantified.

2.2.2. Topsoil

Topsoil data were obtained from a 1:50,000 land-quality geochemical survey. Samples from 0–20 cm depth were collected in accordance with the Specifications for Geochemical Evaluation of Land Quality (DZ/T 0295–2016) [22]. Each sample comprised three to five subsamples and was placed in a clean cloth bag. The western Yuanzhou dataset contained 7411 georeferenced topsoil samples, which were used to establish local soil references around deposition sites.

2.2.3. Irrigation Water and Fertilizers

During the 2019 growing season, 91 irrigation water samples were collected: 56 from rivers, seven from impoundments, four from collection wells, and 24 from reservoirs. Sampling covered the beginning, middle, and end of the irrigation period. Water was collected in 1000 mL plastic bottles, preserved with HNO_3, and submitted for analysis.

In May 2019, 55 fertilizer samples, each weighing approximately 1.0–1.5 kg, were collected. Based on the field records, the samples were divided into six product groups: compound and other fertilizers ($n = 23$), nitrogen fertilizers ($n = 12$), phosphate fertilizers ($n = 11$), organic fertilizers ($n = 4$), potassium fertilizers ($n = 3$), and sulfur fertilizers ($n = 2$). Of these samples, 46 were collected in the valley plain, one in the red-bed hilly area, and eight in the loess hilly area.

2.2.4. Crops and Percolating Water

We collected 313 maize and 164 potato samples, mainly during the September–October harvest seasons of 2019 and 2020. Fields with relatively uniform crop growth were selected, avoiding obvious local pollution sources, field ridges, and abnormal plants. Sampling points followed field diagonals, with crops collected from multiple quadrats. Sampling area and crop fresh and dry weights were recorded. Corresponding tissues from the sampling points were combined into representative samples; grain or tubers were processed separately from other tissues. Maize grain was air-dried in a well-ventilated, uncontaminated setting before analysis, and adhering soil was washed from potato tubers before submission.

Seventeen percolating-water collectors were installed in western Yuanzhou. Each site was observed for approximately one month, with collection periods falling between August and October 2020; 10 valid water samples were obtained. Installation involved excavating pits approximately 80 cm deep and placing collection containers approximately 60 cm high inside them. The containers incorporated plastic mesh, a river-sand layer approximately 50 mm thick, and a plastic partition. Collected water was withdrawn through polypropylene tubing using a manual vacuum pump. Samples were acidified with 5 mL of HNO_3 diluted 1:1 (v/v), sealed, and submitted for analysis.

2.3. Chemical Analysis and Quality Control

All samples were analyzed at the Inner Mongolia Institute of Mineral Experimental Research. Se was determined by hydride generation–atomic fluorescence spectrometry (HG-AFS; Haiguang Instruments Co., Ltd., Beijing, China). HNO_3, HF, $HClO_4$, HCl, H_2O_2 and KBH_4 were obtained from Sinopharm Chemical Reagent Co., Ltd. (Shanghai, China). Sep-

arate preparation procedures were used for survey soils, atmospheric deposition particles and fertilizers, and crop tissues.

For survey soil Se, samples were decomposed with HNO_3–$HClO_4$. Higher-valence Se was reduced in HCl solution before reaction with KBH_4 to generate the volatile hydride, which was transported in argon for fluorescence measurement. For the neighboring-soil element data, Cd was measured by graphite-furnace atomic absorption spectrometry (GF-AAS; M6 Mk2, Thermo Fisher Scientific, Waltham, MA, USA), Pb by ICP-MS (XSERIES 2, Thermo Fisher Scientific, Waltham, MA, USA), and Zn, Cr and Ni by X-ray fluorescence spectrometry (XRF; ZSX Primus series, Rigaku Corporation, Tokyo, Japan), as specified in the survey analytical scheme.

For Se in deposition particles and fertilizers, a 0.5000 g aliquot was wetted with water and digested in a PTFE crucible with 10 mL HNO_3, 10 mL HF and 1 mL $HClO_4$. Heating began at low temperature and did not exceed 200 °C. After the white fumes had just dissipated, the temperature was reduced to 140 °C, 10 mL HCl (1 + 1, v/v) was added, and heating continued for 10 min. After cooling, the solution was transferred to a 50 mL tube, 5 mL iron–salt solution was added, and the mixture was diluted to volume. Se was measured by HG-AFS using KBH_4 as the reductant and HCl (2 + 8, v/v) as the carrier solution.

For particulate Cd and Pb, a separate 0.2000 g aliquot was decomposed with 10 mL HNO_3, 10 mL HF and 3 mL $HClO_4$ on a hotplate at 250 °C. After removal of perchloric acid fumes, 8 mL aqua regia was added to dissolve the residue; the digest was subsequently diluted for ICP-MS. Particulate Zn, Cr and Ni were determined by ICP-OES (NCS Testing Technology Co., Ltd., Beijing, China) after HNO_3–HF–$HClO_4$ decomposition, dissolution with diluted aqua regia and dilution to 25 mL.

For crop Se, 0.2000 g of dry tissue was digested with high-purity HNO_3 and H_2O_2 in a closed microwave vessel. The digest was evaporated to a small volume, cooled and diluted to 10 mL with ultrapure water. A 2.5 mL aliquot was mixed with 1 mL HCl, diluted to 5 mL and analyzed by AFS. This matrix-specific preparation followed the laboratory procedure for plant samples under DZ/T 0253.1–4–2014.

Irrigation-water Se was determined by atomic fluorescence spectrometry under HJ 694–2014.

Survey soil method performance was evaluated using 12 Chinese national first-class certified reference materials: GBW07401–GBW07408 (GSS-1–GSS-8) and GBW07423–GBW07426 (GSS-9–GSS-12), each measured 12 times. For Se, relative standard deviations (RSDs) ranged from 3.19% to 7.84%, and absolute logarithmic concentration deviations (ΔlgC) ranged from 0.000 to 0.029. RSD describes dispersion among repeated measurements; ΔlgC is the absolute difference between the base-10 logarithms of the mean measured and certified concentrations. Routine soil quality control included certified reference materials and blind duplicate samples.

The Se detection limit for percolating water was 0.1 μg L^{-1}. Three of the 10 samples exceeded this limit. The remaining samples were assigned half the detection limit (0.05 μg L^{-1}) for calculations.

2.4. Comparison of Elemental Composition Between Deposition Particles and Neighboring Topsoils

A 3 km radius buffer was established around each deposition site, and the median concentration of each element in topsoil samples within the buffer was used as the local soil reference. The particle-to-soil concentration ratios were calculated using Equation (1):

$$R_{i,j} = \frac{C_{i,j,\mathrm{dep}}}{C_{i,j,\mathrm{soil}}} \quad (1)$$

where i and j denote the element and deposition site, respectively; $C_{i,j,\mathrm{dep}}$ is the concentration of element i in deposition particles; and $C_{i,j,\mathrm{soil}}$ is its median concentration in topsoils within

3 km of site *j*. Both concentrations are expressed in mg kg^{-1}. The ratio $R_{i,j}$ is dimensionless; values above and below 1 indicate higher and lower concentrations in deposition particles than in neighboring topsoils, respectively.

2.5. Cropland Se Inputs and Irrigation Sensitivity

2.5.1. Atmospheric Particulate Se Deposition

Annual particulate deposition mass and the corresponding Se flux per unit area were calculated from particle dry mass, collector opening area, and observation duration. The treatment of atmospheric deposition as a cropland Se input follows previous agricultural budget studies [11–13]:

$$M_{\mathrm{dep}} = 10^4 \times \frac{m}{A \times T} \quad (2)$$

$$F_{\mathrm{dep}} = 10^{-3} \times C_{\mathrm{dep}} \times M_{\mathrm{dep}} \quad (3)$$

where m is the particulate dry mass collected during the observation period (kg); A is the effective collector opening area (0.036644 m^2); T is the observation duration (yr; 1 yr in this study); M_{dep} is annual particulate deposition mass (kg ha^{-1} yr^{-1}); C_{dep} is particulate Se concentration (mg kg^{-1}); and F_{dep} is the annual particulate Se deposition flux (g ha^{-1} yr^{-1}).

2.5.2. Fertilizer and Irrigation Se Inputs

Fertilizer Se inputs were calculated from fertilizer Se concentrations and annual application rates, following agricultural element budget approaches [12,23]:

$$F_{\mathrm{fer}} = 10^{-3} \times C_{\mathrm{fer}} \times q_{\mathrm{fer}} \quad (4)$$

where C_{fer} is fertilizer Se concentration (mg kg^{-1}), q_{fer} is annual product application (kg ha^{-1} yr^{-1}), and F_{fer} is standardized fertilizer Se input (g ha^{-1} yr^{-1}). A farmer-informed rate of 750 kg ha^{-1} yr^{-1} was used to standardize the Se input of each fertilizer product, with products evaluated separately. Irrigation Se inputs were calculated from water Se concentration and a prescribed annual water volume [12,15]:

$$F_{\mathrm{irr}}(x,q) = 10^{-3} \times C_{\mathrm{irr}}(x) \times Q(q) \quad (5)$$

$$Q(q) = 15q \quad (6)$$

where x denotes spatial location; C_{irr} is irrigation-water Se concentration (μg L^{-1}); q and Q denote annual irrigation volumes in m^3 mu^{-1} yr^{-1} and m^3 ha^{-1} yr^{-1}, respectively; and F_{irr} is annual irrigation Se input (g ha^{-1} yr^{-1}). The Chinese area unit mu equals 1/15 ha. The Ningxia Water Resources Bulletin (2020), published in 2021, reports agricultural consumptive water use of 142 m^3 mu^{-1} for Guyuan City in 2020 [24]. Its numerical equivalent, 2130 m^3 ha^{-1} yr^{-1}, was adopted as the irrigation-volume parameter for the reference scenario.

2.5.3. Atmospheric Contributions Under Irrigation Scenarios

The relative contribution of atmospheric deposition was calculated for each raster cell using the three quantified external Se inputs: atmospheric particulate deposition, irrigation, and fertilization:

$$P_{\mathrm{dep}}(x,q) = 100 \times \frac{F_{\mathrm{dep}}(x)}{F_{\mathrm{dep}}(x) + F_{\mathrm{irr}}(x,q) + F_{\mathrm{fer}}(x)} \quad (7)$$

P_{dep} is expressed as a percentage and was calculated for common valid dryland cells with data for all three inputs. Four annual irrigation volumes were evaluated: 2130, 1200, 750 and 0 m^3 ha^{-1} yr^{-1}. The supplemental irrigation references of 1200 and 750 m^3 ha^{-1} yr^{-1} correspond to maize and potato irrigation amounts of 80 and 50 m^3 mu^{-1} reported in the

2023 Guomiao Reservoir project report [25]. These volumes define comparison scenarios rather than observed field irrigation during the monitoring period.

Each irrigation volume was applied uniformly across the same valid dryland cells, while atmospheric deposition, fertilizer inputs and irrigation-water Se concentrations were held constant. We calculated the median atmospheric contribution, the area and percentage with contributions ≥25%, and the percentage with contributions >50%. The zero-irrigation scenario represents a limiting comparison retaining atmospheric and fertilizer inputs.

Sensitivity analyses evaluated irrigation volumes continuously from 0 to 4260 m^3 ha^{-1} yr^{-1} and fertilizer application rates of 375, 750 and 1125 kg ha^{-1} yr^{-1}. Joint parameter tests additionally varied irrigation-water Se concentrations. Detailed settings and results are provided in the Supplementary Materials; interpolation-model and site-influence analyses are described in Section 2.8.

2.6. Estimation of Cropland Se Outputs

2.6.1. Crop Harvest Export

Se export through maize grain and potato tuber harvest was calculated separately from Se concentrations and annual yields, following agricultural Se cycling and budget studies [11–13]. Both concentrations and yields were expressed on a dry weight basis. Harvest export included only maize grain and potato tubers, with other residues assumed to return to the field. No harvest export was estimated for the loess hilly area because corresponding crop samples were unavailable.

$$F_{\mathrm{harv},c} = 10^{-3} \times C_{\mathrm{crop},c} \times Y_c \quad (8)$$

where c denotes maize or potato; $C_{\mathrm{crop},c}$ is Se concentration in grain or tubers (mg kg^{-1}); Y_c is the annual dry weight yield of the corresponding crop (kg ha^{-1} yr^{-1}); and $F_{\mathrm{harv},c}$ is the harvest Se export flux (g ha^{-1} yr^{-1}).

2.6.2. Observed-Period Percolating Water Flux

The Se flux in percolating water was calculated separately for each sample over its approximately one-month collection period between August and October 2020:

$$F_{\mathrm{leach,obs},j} = 0.01 \times \frac{C_j \times V_j}{A_{\mathrm{L}}} \quad (9)$$

where j denotes an individual percolating water sample, C_j is its Se concentration (μg L^{-1}), V_j is its collected water volume (L), A_{L} is the effective collection area (0.070686 m^2), and $F_{\mathrm{leach,obs},j}$ is the Se mass collected per hectare during that sample's observation period (g ha^{-1} per observation period). The seven nondetects were assigned half the detection limit (0.05 μg L^{-1}) for the central calculation; assigning 0 and the detection limit (0.1 μg L^{-1}) provides substitution bounds.

2.6.3. Soil Se Volatilization

The illustrative volatilization calculation follows the stock-based approach used by Yu et al. [13], who adopted an annual relative volatilization coefficient of 0.024% based on Wang [26]:

$$F_{\mathrm{vol}} = f \times S_{\mathrm{Se}} \quad (10)$$

where S_{Se} is reference topsoil Se stock (g ha^{-1}), f is the literature-derived annual relative volatilization coefficient of 0.024% yr^{-1} (2.4×10^{-4} yr^{-1}), and F_{vol} is the illustrative volatilization flux (g ha^{-1} yr^{-1}).

2.7. Comparison of Annual Atmospheric Input with Topsoil Se Stocks

Se stocks per unit area were estimated for the 0–20 cm topsoil using a uniform bulk density. The ratio of annual atmospheric particulate Se deposition to these stocks was then calculated:

$$M_{soil} = 10^7 \times \rho \times z \quad (11)$$

$$S_{Se} = 10^{-3} \times C_{soil} \times M_{soil} \quad (12)$$

$$Q_{dep} = 100 \times \frac{F_{dep}}{S_{Se}} \quad (13)$$

where ρ is soil bulk density (g cm^{-3}), z is thickness (m), M_{soil} is soil mass per hectare (kg ha^{-1}), C_{soil} is soil Se concentration (mg kg^{-1}), S_{Se} is reference stock (g ha^{-1}), and Q_{dep} is deposition-to-stock ratio (% yr^{-1}). Because site-specific bulk densities were not measured, a uniform reference density of 1.30 g cm^{-3}, supported by regional field measurements [27], and $z = 0.20$ m were used, giving $M_{soil} = 2.60 \times 10^6$ kg ha^{-1} and $S_{Se} = 2600 C_{soil}$. Deposition fluxes were extracted at 5481 topsoil sampling locations within dryland or irrigated cropland polygons. Deposition-to-stock ratios were calculated at these locations and summarized as medians by land use and geomorphic unit.

2.8. Statistical and Spatial Analyses

Data were organized in WPS Office 12.1.0.29690 (Kingsoft Office, Beijing, China) and analyzed using IBM SPSS Statistics 23 (IBM Corp., Armonk, NY, USA), ArcGIS 10.8 (Esri, Redlands, CA, USA) and Python 3.12 (Python Software Foundation, Beaverton, OR, USA). Descriptive statistics included means, medians and interquartile ranges, with sample-based and raster-based summaries distinguished. Three site-level Spearman correlations were evaluated using two-sided t approximations, with Benjamini–Hochberg adjustment across the three tests. Differences in particulate Se concentration and deposition flux among geomorphic units were assessed using permutation-based Kruskal–Wallis tests with 19,999 permutations (seed 4682607) and Holm adjustment across the two tests. These comparisons were exploratory given the small groups (7, 5 and 4 sites) and possible spatial dependence.

Spatial interpolation used IDW with a power of 2, the 12 nearest locations, no barriers and a cell size of 156.81 m in CGCS2000 three-degree Gauss–Krüger Zone 35. Concentrations at coincident sampling locations were averaged before interpolation, yielding 16 distinct deposition locations, 90 irrigation water locations and 14 fertilizer locations. Atmospheric contribution statistics were calculated over a common valid dryland mask. Land use was assigned by each cell center, and areas were calculated from cell counts and projected cell area.

Interpolation performance was evaluated using leave-one-location-out cross-validation, with all coincident samples excluded together. Prediction errors were summarized using MAE, RMSE and bias. Sensitivity analyses compared nine combinations of IDW powers (1, 2 and 3) and neighborhood sizes (4, 8 and 12 locations), together with delete-one-location analyses. The influence of the neighboring soil reference was examined using 1, 3 and 5 km buffers. Detailed procedures and results are provided in the Supplementary Materials.

Generative AI was used to assist with coding (see Acknowledgments).

3. Results

3.1. Composition of Se and Associated Elements in Deposition Particles

Particulate Se concentrations at the 16 deposition sites ranged from 0.387 to 0.682 mg kg^{-1}, with a median of 0.557 mg kg^{-1}. Relative to the median Se concentration in topsoils

within 3 km of each site, particle-to-soil Se concentration ratios ranged from 2.43 to 4.86 (median: 3.59) and exceeded 1 at all sites. Associated elements showed contrasting patterns: median ratios were 4.23, 2.67, and 1.40 for Cd, Zn, and Pb, respectively, compared with 0.75 for Cr and 0.77 for Ni (Figure 2).

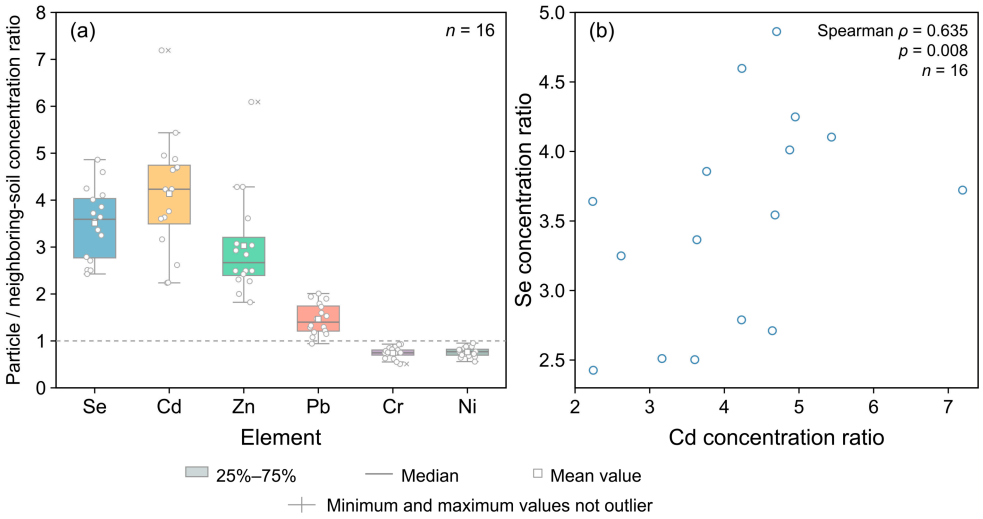


Figure 2. Elemental concentration ratios of deposited particles to neighboring topsoils at 16 sites. (**a**) Distributions of Se, Cd, Zn, Pb, Cr and Ni concentration ratios. Open circles represent individual sites, and crosses (×) indicate outliers. The dashed horizontal line denotes a concentration ratio of 1. (**b**) Relationship between Cd and Se concentration ratios at the same sites. Spearman's ρ and the unadjusted two-sided *p*-value are shown.

Se and Cd particle-to-soil concentration ratios were positively associated across the 16 deposition sites (Spearman ρ = 0.635; nominal $p = 0.008$; Benjamini–Hochberg-adjusted $p = 0.025$ across the three stated correlation tests). Figure 2 shows the elemental concentration-ratio distributions and the site-level association.

Using 1, 3 and 5 km soil buffers, median Se concentration ratios were 3.37, 3.59 and 3.72, respectively; every site remained above 1 (Supplementary Materials).

3.2. Major Cropland Se Inputs and Their Spatial Variation

Atmospheric deposition. Recovered particulate mass ranged from 848.66 to 2723.32 kg ha^{-1} yr^{-1} (median: 1379.47), equivalent to 84.87–272.33 g m^{-2} yr^{-1}. Se fluxes ranged from 0.501 to 1.715 g ha^{-1} yr^{-1} (median: 0.710). Valley-plain, red-bed-hill and loess-hill sites had mean fluxes of 1.01, 0.79 and 0.61 g ha^{-1} yr^{-1} and medians of 0.947, 0.674 and 0.627, respectively (Figure 3; Table S2). The mean concentrations were 0.53, 0.52 and 0.58 mg kg^{-1}. Exploratory differences among units were not significant after Holm adjustment for the two tests: flux H = 6.280, nominal permutation $p = 0.031$, adjusted $p = 0.063$; concentration H = 0.962, nominal and adjusted $p = 0.642$.

Annual deposition flux had little association with particulate Se concentration (Spearman ρ = −0.068; nominal and adjusted $p = 0.803$). Its association with the Se particle-to-soil concentration ratio was negative (ρ = −0.544; nominal $p = 0.029$; adjusted $p = 0.044$). Ershilipu had the highest concentration ratio (4.86) and an annual flux of 0.674 g ha^{-1} yr^{-1}; Malu Village had the highest flux (1.715 g ha^{-1} yr^{-1}). Figure 4a maps the collector-derived deposition estimates.

Fertilizer inputs. Se concentrations in the 55 fertilizer samples ranged from 0.02 to 3.64 mg kg^{-1}, with a mean of 0.15 mg kg^{-1}. Standardization to a uniform fertilizer application rate of 750 kg ha^{-1} yr^{-1} yielded a mean annual Se input of 0.11 g ha^{-1} yr^{-1}.

Sample-based mean inputs for the valley plain, red-bed hilly area, and loess hilly area were 0.13, 0.02, and 0.03 g ha^{-1} yr^{-1}, respectively. Organic fertilizers sampled in the valley plain had the highest mean Se concentration (1.17 mg kg^{-1}), corresponding to a standardized flux of 0.87 g ha^{-1} yr^{-1}. Within the valley plain, mean concentrations in potassium and phosphate fertilizers were 0.26 and 0.15 mg kg^{-1}, corresponding to fluxes of 0.19 and 0.11 g ha^{-1} yr^{-1}, respectively. Sample counts, Se concentrations, and standardized fluxes by field-record product group are presented in Table 1; their spatial distribution is shown in Figure 4b.

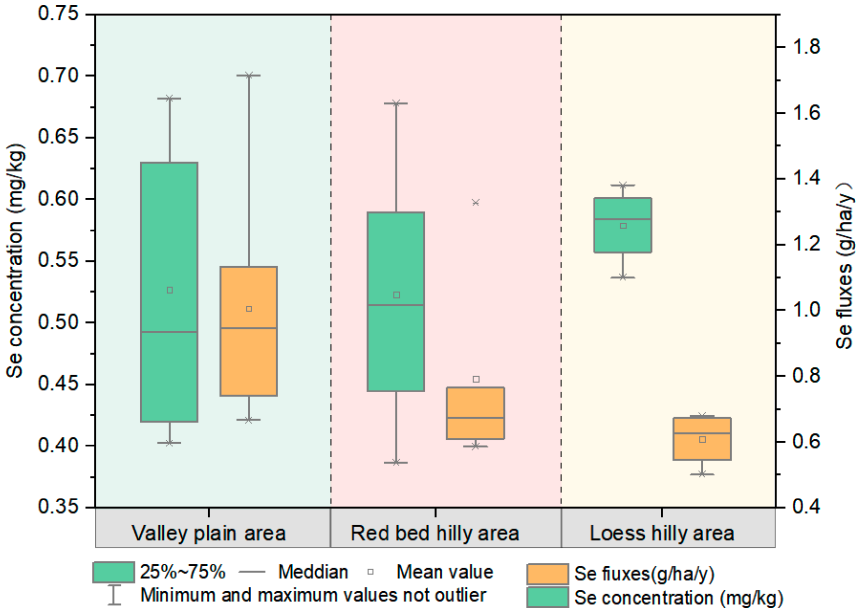


Figure 3. Se concentrations in atmospheric deposition particles and corresponding annual deposition fluxes across the major geomorphic units. Crosses (×) beyond the whiskers indicate outliers.

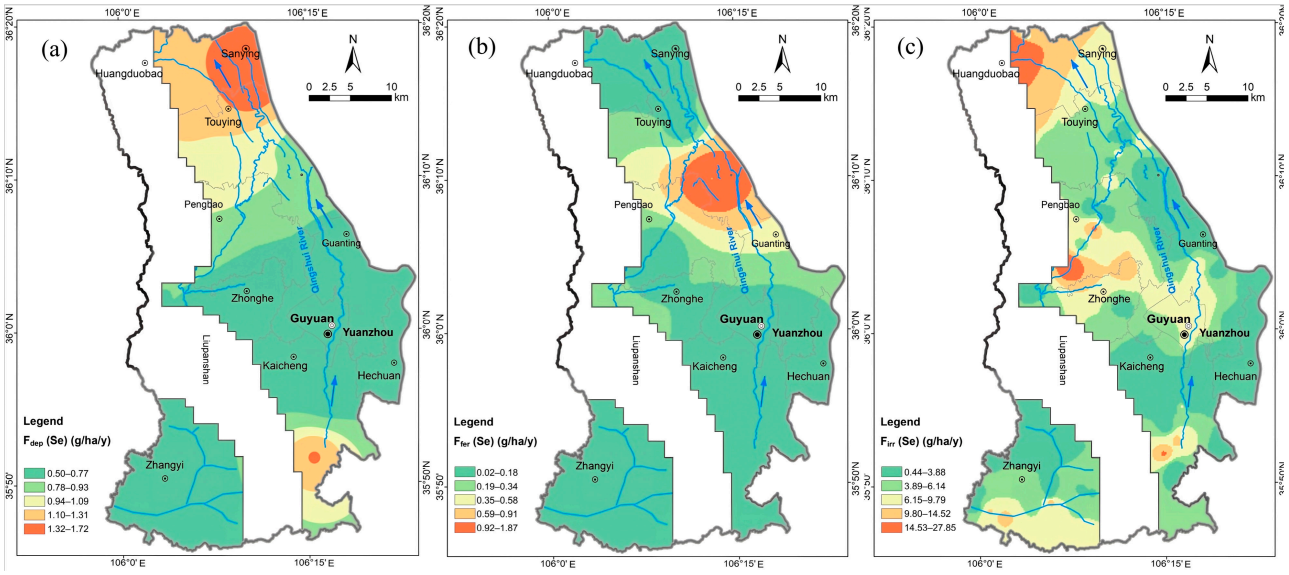


Figure 4. Spatial distributions of annual Se input fluxes estimated using IDW: (**a**) collector-derived particulate Se deposition, (**b**) fertilizer Se input standardized to 750 kg ha^{-1} yr^{-1}, and (**c**) irrigation Se input at a prescribed irrigation volume of 2130 m^3 ha^{-1} yr^{-1}. All fluxes are expressed in g ha^{-1} yr^{-1}. Blue arrows indicate river flow direction.

Table 1. Se concentrations and standardized annual input fluxes of fertilizer samples by field-record product group.

Geomorphic Unit	Fertilizer Group	*n*	Maximum		Minimum		Mean	
			Se [1]	Flux [2]	Se [1]	Flux [2]	Se [1]	Flux [2]
VP	Nitrogen	9	0.05	0.04	0.03	0.02	0.04	0.03
VP	Compound and other fertilizers	20	0.11	0.09	0.02	0.01	0.04	0.03
VP	Potassium	3	0.69	0.52	0.04	0.03	0.26	0.19
VP	Phosphate	9	1.00	0.75	0.02	0.02	0.15	0.11
VP	Sulfur	1	0.05	0.04	0.05	0.04	0.05	0.04
VP	Organic	4	3.64	2.73	0.21	0.15	1.17	0.87
VP	Subtotal	46	3.64	2.73	0.02	0.01	0.17	0.13
RBH	Compound and other fertilizers	1	0.03	0.02	0.03	0.02	0.03	0.02
LH	Nitrogen	3	0.03	0.03	0.03	0.02	0.03	0.02
LH	Compound and other fertilizers	2	0.04	0.03	0.03	0.03	0.04	0.03
LH	Phosphate	2	0.05	0.04	0.04	0.03	0.04	0.03
LH	Sulfur	1	0.02	0.01	0.02	0.01	0.02	0.01
LH	Subtotal	8	0.05	0.04	0.02	0.01	0.03	0.03
All samples		55	3.64	2.73	0.02	0.01	0.15	0.11

Note: The "Compound and other fertilizers" category follows the original field-record grouping and includes nitrogen–phosphorus (NP) and nitrogen–phosphorus–potassium (NPK) fertilizers, calcium ammonium nitrate, boron fertilizers and multi-element nutrient products. Nutrient formulations varied among the sampled products. Fluxes were standardized to 750 kg ha^{-1} yr^{-1}; product-specific application rates were unavailable. The fertilizer input estimate for the red-bed hilly area was based on one sample. VP, valley plain; RBH, red-bed hilly area; LH, loess hilly area. [1] Se concentration (mg kg^{-1}); [2] standardized Se input flux (g ha^{-1} yr^{-1}).

Irrigation inputs. Mean Se concentration in the 91 sampled sources was 2.58 μg L^{-1}. At Q = 2130 m^3 ha^{-1} yr^{-1}, the sample mean input was 5.51 g ha^{-1} yr^{-1}. Mean concentrations and prescribed inputs were 3.73 μg L^{-1} and 7.93 g ha^{-1} yr^{-1} for rivers, 1.14 and 2.43 for impoundments, 0.90 and 1.92 for collection wells, and 0.63 and 1.33 for reservoirs (Table 2).

Table 2. Se concentrations in irrigation-water samples and estimated input fluxes at the reference scenario irrigation volume.

Water Source	Geomorphic Unit	*n*	Maximum		Minimum		Mean	
			Se [1]	Flux [2]	Se [1]	Flux [2]	Se [1]	Flux [2]
River	Total	56	13.20	28.12	0.70	1.49	3.73	7.93
River	VP	32	13.20	28.12	0.70	1.49	4.10	8.73
River	RBH	17	7.20	15.34	0.70	1.49	3.20	6.82
River	LH	7	5.50	11.71	0.90	1.92	3.30	7.03
Collection well	Total	4	1.70	3.62	0.20	0.43	0.90	1.92
Collection well	VP	2	1.00	2.13	0.20	0.43	0.60	1.28
Collection well	RBH	2	1.70	3.62	0.70	1.49	1.20	2.56

Table 2. *Cont.*

Water Source	Geomorphic Unit	*n*	Maximum		Minimum		Mean	
			Se [1]	Flux [2]	Se [1]	Flux [2]	Se [1]	Flux [2]
Impoundment	Total	7	2.10	4.47	0.40	0.85	1.14	2.43
Impoundment	RBH	3	1.10	2.34	0.70	1.49	0.87	1.85
Impoundment	LH	4	2.10	4.47	0.40	0.85	1.35	2.88
Reservoir	Total	24	1.30	2.77	0.20	0.43	0.63	1.33
Reservoir	VP	11	1.30	2.77	0.20	0.43	0.67	1.43
Reservoir	RBH	10	1.00	2.13	0.40	0.85	0.65	1.38
Reservoir	LH	3	0.40	0.85	0.30	0.64	0.37	0.78
All samples		91	13.20	28.12	0.20	0.43	2.58	5.51

Note: Irrigation inputs were estimated at the reference scenario volume of 2130 m^3 ha^{-1} yr^{-1} (142 m^3 mu^{-1} yr^{-1}), using the numerical equivalent of the reported agricultural consumptive use indicator [24]. Values are sample-based statistics; the spatial contribution analyses use GIS raster zonal statistics. VP, valley plain; RBH, red-bed hilly area; LH, loess hilly area. [1] Se concentration (μg L^{-1}); [2] estimated Se input flux (g ha^{-1} yr^{-1}).

At the prescribed reference volume, sample-based mean irrigation inputs were 6.61, 4.39 and 4.50 g ha^{-1} yr^{-1} in the valley plain, red-bed hills and loess hills; corresponding medians were 5.112, 2.343 and 3.195. In each unit, both sample means and sample medians ranked prescribed irrigation above deposition and standardized fertilizer input (Table S2; Figure S1).

3.3. Spatial Variation in Atmospheric Contributions Under Reference and Supplemental Irrigation Scenarios

At Q = 2130 m^3 ha^{-1} yr^{-1} and q_{fer} = 750 kg ha^{-1} yr^{-1}, the common valid dryland area was 73,008.54 ha. The median atmospheric share was 14.91%; shares ≥25% covered 2503.12 ha (3.43%). No valid dryland cell had a share >50% (Table 3).

Table 3. Atmospheric Se contributions over the common valid dryland extent under reference and locally informed supplemental irrigation scenarios.

Annual Dryland Irrigation (m^3 ha^{-1} yr^{-1})	Median Atmospheric Contribution (%)	Area with Contribution ≥ 25% (ha)	Area with Contribution ≥ 25% (%)	Area with Contribution > 50% (%)
2130	14.91	2503.12	3.43	0.00
1200	22.85	26,344.25	36.08	0.21
750	30.92	55,287.52	75.73	1.58
0	80.74	73,008.54	100.00	98.32

Note: The common valid dryland area is 73,008.54 ha. Q = 2130 m^3 ha^{-1} yr^{-1} is the reference scenario parameter derived from the regional consumptive-use indicator [24]. Q = 1200 and 750 correspond to the maize and potato supplemental-irrigation amounts reported for the Guomiao Reservoir district [25]; each was applied separately to the entire valid dryland extent. Q = 0 is the zero-irrigation limiting case. Areas were calculated directly from raster cell counts; areas and percentages were rounded independently.

The continuous comparisons in Figure 5 place the selected irrigation references on curves spanning Q = 0–4260 m^3 ha^{-1} yr^{-1}. Both median share and the area above the ≥25% threshold varied with prescribed water volume and fertilizer rate.

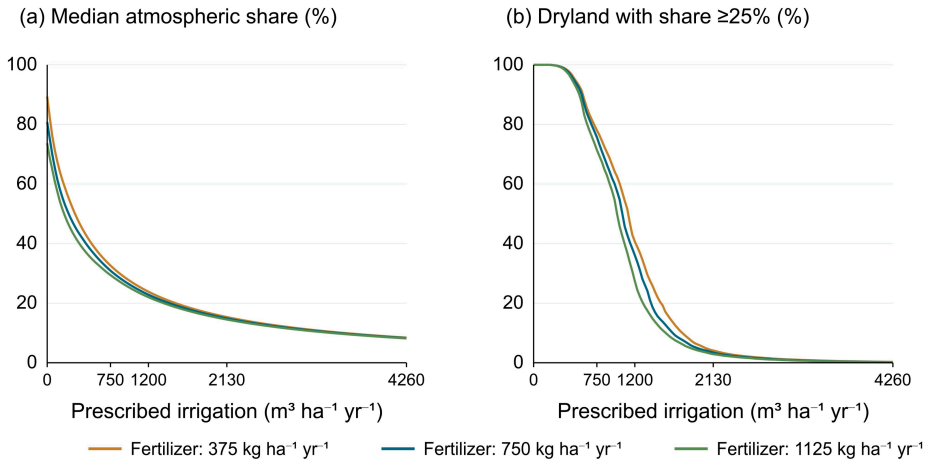


Figure 5. Continuous dependence of (**a**) median atmospheric share and (**b**) dryland area with share ≥25% on prescribed water volume, at three standardized fertilizer rates. Deposition, irrigation-water Se concentrations and the dryland mask are otherwise fixed.

The spatial distributions of deposition flux and conditional atmospheric share differed (Figures 4a and 6).

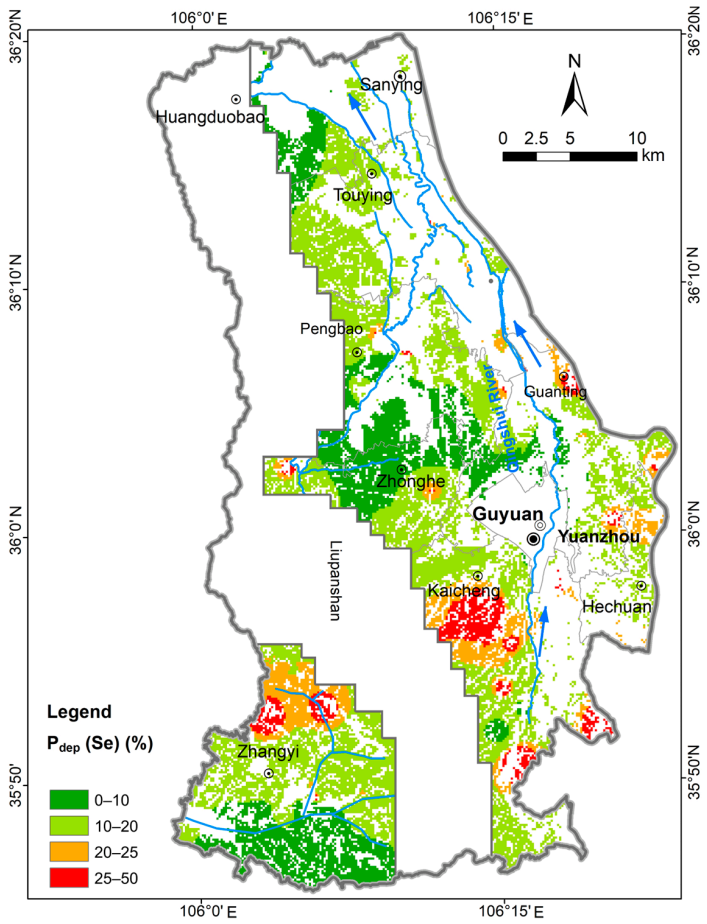


Figure 6. Atmospheric particulate Se contribution to the three quantified Se inputs at Q = 2130 m^3 ha^{-1} yr^{-1} and a standardized fertilizer rate of 750 kg ha^{-1} yr^{-1}. P_{dep} denotes the percentage contribution of atmospheric particulate Se deposition to the sum of atmospheric, irrigation and fertilizer Se inputs, as defined in Equation (7). Only common valid dryland cells are classified; white indicates areas outside that mask. The gray outline delineates the regional boundary. Blue arrows indicate river flow direction.

Across the assessed dryland cells in the valley plain and loess hilly area, mean particulate Se deposition fluxes were 0.901 and 0.668 g ha^{-1} yr^{-1}, respectively. Under the reference irrigation scenario, the corresponding median atmospheric contributions were 11.43% and 15.21%.

Under the same reference scenario, raster-based mean irrigation Se input fluxes were 7.185 g ha^{-1} yr^{-1} in the valley plain and 3.883 g ha^{-1} yr^{-1} in the loess hilly area. Assessed dryland in the loess hilly area covered 10,514 ha, accounting for 14.4% of the total assessed dryland. Of this area, 1453 ha had atmospheric contributions ≥ 25%, accounting for 58.1% of all assessed dryland meeting that threshold.

At Q = 1200 m^3 ha^{-1} yr^{-1}, the median atmospheric contribution was 22.85%, and contributions ≥ 25% covered 26,344.25 ha (36.08%). At Q = 750 m^3 ha^{-1} yr^{-1}, the median was 30.92%, and the corresponding area was 55,287.52 ha (75.73%). Contributions > 50% covered 0.21% and 1.58% of assessed dryland, respectively. In the Q = 0 limiting case, the median contribution was 80.74%; all assessed dryland had contributions ≥ 25%, and 98.32% had contributions > 50% (Table 3).

At Q = 2130 m^3 ha^{-1} yr^{-1}, the nine IDW alternatives yielded median atmospheric contributions of 14.02–15.91% and areas with contributions ≥ 25% covering 0.63–15.65% of assessed dryland. At the same irrigation volume, the joint sensitivity analysis of irrigation-water Se concentration and fertilizer rate yielded medians of 10.46–25.95% and corresponding dryland percentages of 0.70–55.92%. Figure 5 shows the continuous parameter comparisons; detailed interpolation model and site influence results are provided in the Supplementary Materials.

3.4. Estimated Se Outputs and Comparison with Atmospheric Deposition

Across the crop-sampled valley plain and red-bed hilly area, pooled estimates of harvest Se export were 0.47 g ha^{-1} yr^{-1} for maize grain and 0.269 g ha^{-1} yr^{-1} for potato tubers. Corresponding crop-specific exports were 0.54 and 0.30 g ha^{-1} yr^{-1} in the valley plain and 0.21 and 0.24 g ha^{-1} yr^{-1} in the red-bed hilly area. Pooled values are sample-count-weighted means: maize samples comprised 243 from the valley plain and 70 from the red-bed hilly area, and potato samples comprised 73 and 91, respectively. Mean annual atmospheric particulate Se deposition in the valley plain and red-bed hilly area was 1.01 and 0.79 g ha^{-1} yr^{-1}, respectively, exceeding each crop-specific harvest export in the corresponding geomorphic unit (Figure 7 and Table 4).

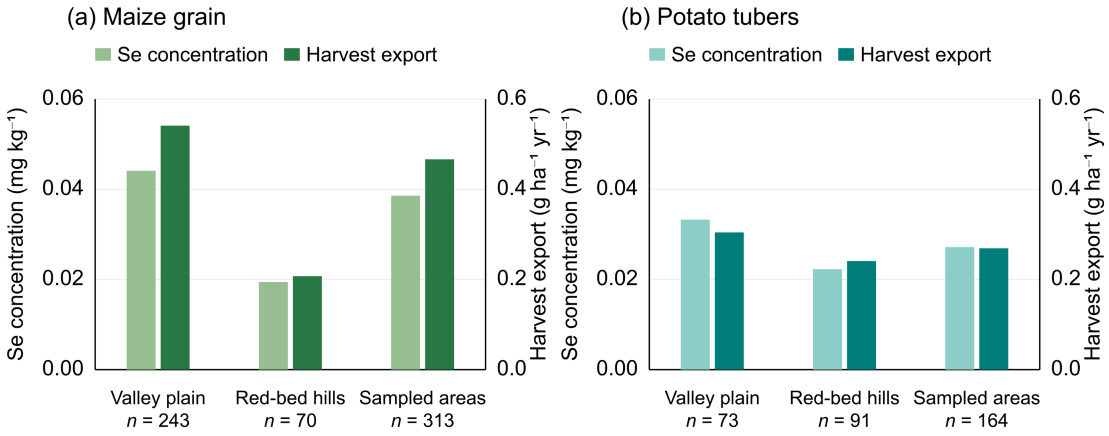


Figure 7. Mean Se concentrations and estimated harvest exports for (**a**) maize grain and (**b**) potato tubers. "Sampled areas" denotes the pooled sample mean for the valley plain and red-bed hilly area, weighted by the numbers of samples shown below each group; the loess hilly area is excluded. Left axes show Se concentration (mg kg^{-1}), and right axes show harvest export (g ha^{-1} yr^{-1}).

Table 4. Annual atmospheric particulate Se input and separately estimated Se output fluxes by geomorphic unit. Numerical columns are in g ha^{-1} yr^{-1}.

Se input or Output Pathway	Valley Plain (g ha^{-1} yr^{-1})	Red-Bed Hilly Area (g ha^{-1} yr^{-1})	Loess Hilly Area (g ha^{-1} yr^{-1})
Atmospheric particulate Se deposition (input)	1.01	0.79	0.61
Maize grain harvest (export)	0.54	0.21	—
Potato tuber harvest (export)	0.30	0.24	—
Soil Se volatilization (literature parameter estimate)	0.12	0.10	0.09

Note: Harvest Se exports include maize grain and potato tubers, with crop residue return assumed; —, unavailable crop data. Volatilization fluxes were estimated using a literature-derived coefficient. All fluxes are presented as positive magnitudes.

Over the approximately one-month percolation observation, three detected samples yielded 7.972, 0.248 and 0.150 g ha^{-1} per observation period. The 7.972 value was from XS01 near a grassland–cropland boundary. The seven nondetects yielded 0.0004–0.0106 g ha^{-1} using half the detection limit; their individual 0-to-detection-limit bounds extended from 0 to at most 0.0212 g ha^{-1}. Sample-level Se concentrations and collected water volumes are provided in Supplementary Data S1. These observations are excluded from the annual comparison in Table 4.

Estimated soil Se volatilization fluxes were approximately 0.12, 0.10 and 0.09 g ha^{-1} yr^{-1} for the valley plain, red-bed hilly area and loess hilly area, respectively, with an overall estimate of approximately 0.11 g ha^{-1} yr^{-1} (Table 4).

3.5. Annual Atmospheric Input Relative to Topsoil Se Stocks

At the 5481 topsoil locations matched to dryland or irrigated cropland polygons, the median Se stock in the 0–20 cm topsoil was 439.4 g ha^{-1}; medians for dryland and irrigated croplands were 416.0 and 517.4 g ha^{-1}, respectively. The median ratio of annual atmospheric particulate Se deposition to topsoil Se stocks was 0.190% yr^{-1}. Corresponding ratios were approximately 0.198%, 0.189%, and 0.169% yr^{-1} in the valley plain, red-bed hilly area, and loess hilly area, respectively.

4. Discussion

4.1. Selective Se Enrichment in Atmospheric Deposition Particles and Possible Explanations

Se concentrations in deposited particles exceeded those in neighboring topsoils at all 16 sites. Median particle-to-soil concentration ratios also exceeded 1 for Cd, Zn and Pb, whereas those for Cr and Ni were below 1 (Figure 2). These contrasting patterns indicate compositional differences between the deposited material and surrounding bulk topsoil. The positive association between Se and Cd ratios suggests that their relative enrichment varied together across sites. The Se ratio was negatively related to annual deposition flux, while particulate Se concentration showed no significant relationship with flux. These results highlight the distinction between relative enrichment and annual supply: the former depends on both particle and soil concentrations, whereas the latter reflects particle concentration and deposited mass. The correlation patterns, therefore, need to be considered alongside these calculation relationships.

Wind erosion and mineral dust transport are plausible contributors to the deposited material. Soil Se distributions in Yuanzhou have been linked to geological sources, soil formation and hydrological transport [19,20], providing a basis for spatial differences in the material available for resuspension. The local mineral resources plan documents open-pit

extraction of limestone, dolomite and sand [28]. Erosion, extraction, agricultural disturbance and transportation may release particles for subsequent atmospheric transport and deposition. Particle sorting, mineral composition and surface adsorption can redistribute trace elements among particle size fractions [10]. Deposited dust therefore need not reproduce the composition of nearby bulk topsoil, even when some material originates locally. Because the fine fraction of local soil was not separately analyzed, the observed ratios represent concentration contrasts with bulk topsoil and may reflect both particle sorting and source mixing.

Published observations provide regional context for the recovered particle masses. Sun et al. reported monthly dust fluxes of 15–35 g m^{-2} at Lanzhou and 10–25 g m^{-2} at Yuzhong [29], demonstrating substantial dust deposition in the western Loess Plateau. Our annual recovered masses were 84.87–272.33 g m^{-2}. Differences in location, collection interval and collector maintenance, including monthly recovery and water-maintained collectors in the earlier study, limit direct quantitative comparison. Nevertheless, these observations support considering both transported dust and local resuspension when interpreting particulate deposition in this region. Contributions from nearby disturbed surfaces or incidental contamination also warrant consideration because estimated Se flux scales directly with recovered particle mass.

Other atmospheric sources may contribute to Se enrichment. Global models describe Se deposition as the combined outcome of natural sources, anthropogenic emissions and atmospheric transport [2,4,5]. Coal combustion cannot be excluded: Se enrichment in fine fly-ash particles provides a plausible pathway for atmospheric Se transport [30]. Agricultural bulk deposition and speciation studies further illustrate how multiple sources and weather processes influence deposited Se [7,8]. A mixture of mineral dust and aerosols from other sources is, therefore, a plausible explanation for the observed elemental patterns in western Yuanzhou. Quantifying the respective contributions of coal combustion, mining and soil resuspension would require complementary evidence from conservative element normalization, particle mineralogy, source tracers or atmospheric transport analysis.

The annual collectors recovered particulate Se delivered by rainfall and dry deposition. Prolonged exposure may affect particle recovery and Se retention, but replicate collector, field blank and collection efficiency data were unavailable to quantify these effects. Liquid-fraction Se was below the detection limit, but annual filtrate volumes were not retained, preventing calculation of an upper bound on dissolved Se flux (Supplementary Material Section S5). Locally resuspended soil may also contribute to the collected material, so part of the deposition may represent redistribution within the region rather than new Se input from outside it.

4.2. Spatial Variation in Atmospheric Contributions and Their Relationship with Irrigation Inputs

The spatial distribution of atmospheric Se contributions did not fully coincide with that of particulate deposition flux because the contribution depends on the relative magnitudes of the three quantified inputs. Under the reference scenario, the valley plain had higher deposition fluxes than the loess hilly area but lower atmospheric contributions, accompanied by higher estimated irrigation Se inputs. The loess hilly area accounted for a larger proportion of dryland with atmospheric contributions $\geq$ 25% than of the total assessed dryland. Thus, a high atmospheric contribution does not necessarily indicate a high deposition flux; it can also reflect lower irrigation and fertilizer Se inputs. Regional Se budget studies similarly report substantial differences in atmospheric contributions [13–15], although comparisons among regions should consider differences in water use and the input pathways included.

Seasonal rainfall, widespread rainfed farming and varying irrigation practices on the Loess Plateau [31,32] make irrigation an important factor in interpreting these spatial differences. The maize and potato supplemental irrigation amounts reported for the Guomiao Reservoir district [25] provide regional references for examining atmospheric contributions under lower irrigation inputs. Compared with the reference scenario, these lower volumes increased atmospheric contributions and expanded the dryland area where deposition supplied at least one quarter of the quantified Se inputs. Atmospheric deposition remained unchanged across the scenarios; the increase in its share resulted from reduced irrigation-borne Se supply. Consequently, atmospheric deposition can become relatively more important under limited irrigation even without an increase in atmospheric delivery.

The continuous sensitivity analysis showed that atmospheric contributions decreased as irrigation volume increased at all three prescribed fertilizer rates, with more pronounced changes within the lower irrigation range (Figure 5). This response further illustrates how reduced irrigation-borne Se supply increases the relative importance of atmospheric deposition within the quantified inputs. Irrigation-water Se concentration, fertilizer rate and interpolation method also affected the calculated contributions and the area with contributions $\geq 25\%$, with threshold areas particularly sensitive to these changes. Comparisons among irrigation scenarios should therefore be interpreted alongside the sensitivity results, especially when assessing the extent of high-contribution areas. Because field-specific irrigation volumes and fertilizer application records were unavailable for the monitoring period, these results represent atmospheric contributions under the specified input conditions.

4.3. Annual Se Supply from Particulate Deposition and Its Relationship with Soil Stocks

Atmospheric particulate Se deposition provides an annual input comparable in magnitude to Se removal through crop harvest. In the crop-sampled valley plain and red-bed hilly area, mean deposition fluxes exceeded the separately estimated exports through maize grain or potato tubers. These comparisons indicate that atmospheric deposition is an input pathway that warrants inclusion in assessments of annual cropland Se supply, consistent with regional Se budget studies [13,14]. They demonstrate the magnitude of atmospheric supply relative to agricultural removal, while its contribution to crop nutrition depends on subsequent retention, transformation and uptake.

Although atmospheric deposition was appreciable relative to annual harvest export, it represented a small annual addition relative to the existing soil Se inventory. The median ratio of annual particulate deposition to Se stocks in the 0–20 cm topsoil was 0.190% yr^{-1}. These comparisons reflect different timescales: crop harvest represents annual removal, whereas soil stocks integrate inputs, retention and transport over longer periods. Local soil Se distributions are associated with geological sources, soil formation and hydrological transport [19,20], while minerals, organic matter and biogeochemical processes influence the fate of incoming Se [3,33]. Atmospheric deposition can, therefore, contribute to annual Se cycling, while its long-term contribution to soil stocks depends on subsequent retention and export.

Volatilization and leaching are additional pathways of Se loss from croplands. Volatilization fluxes estimated using the literature-derived coefficient were lower than particulate deposition inputs (Table 4) [13,26]. Short-period percolating-water observations showed substantial differences in dissolved Se export among sampling sites, but longer monitoring is needed to determine annual fluxes. Harvest-export comparisons cover only maize grain and potato tubers in the valley plain and red-bed hilly area, with other crop residues assumed to return to the field. Because the pathways were assessed over different periods and areas, these estimates are used to compare input and output magnitudes, without calculating a complete annual Se balance.

5. Conclusions

Atmospheric particulate deposition supplied Se to croplands in western Yuanzhou, with annual collector-derived fluxes of 0.501–1.715 g ha^{-1} yr^{-1}. Deposited particles had higher Se concentrations than neighboring bulk topsoils, indicating relative enrichment potentially associated with particle sorting and source mixing.

Scenario comparisons identified irrigation input as an important factor influencing the relative contribution of atmospheric deposition. At a standardized fertilizer rate of 750 kg ha^{-1} yr^{-1}, reducing prescribed irrigation from 2130 to 750 m^3 ha^{-1} yr^{-1} increased the median atmospheric contribution from 14.91% to 30.92%. Sensitivity analyses further showed that the area with contributions $\geq$ 25% was particularly sensitive to input parameters and interpolation methods.

In the crop-sampled geomorphic units, deposition exceeded the separately estimated exports through grain or tuber harvest, while annual deposition represented a small fraction of existing topsoil Se stocks. These findings highlight atmospheric particulate deposition as a relevant supply pathway in annual cropland Se cycling, with greater relative importance under scenarios with lower irrigation-borne Se inputs.

Supplementary Materials: The following supporting information can be downloaded at: https://www.mdpi.com/article/10.3390/atmos17111141/s1, Supplementary Analyses: Sections S1–S5; Figure S1: Mean irrigation-water Se concentrations and corresponding Se input fluxes across the major geomorphic units; Table S1: Leave-one-location-out cross-validation errors; Table S2: Sample-based Se input summaries; Table S3: Particle-to-soil Se concentration ratios for 1, 3 and 5 km soil-reference buffers; Table S4: Sensitivity ranges for fertilizer rates and irrigation-water Se concentrations; Table S5: Sensitivity ranges across nine IDW alternatives; Supplementary Data S1: Measurement data and derived scenario summaries (Atmosphere_Minimal_Dataset.xlsx). References [13,27] are also cited in the Supplementary Analyses.

Author Contributions: Conceptualization, X.L.; formal analysis, X.L. and Y.D.; investigation, Y.D. and Z.W.; writing—original draft preparation, X.L.; writing—review and editing, Y.D., Z.W., K.L., T.Y. and Z.Y.; supervision, Y.D., K.L., T.Y. and Z.Y.; project administration, T.Y. All authors have read and agreed to the published version of the manuscript.

Funding: This research was supported by the National Natural Science Foundation of China (42607426), the China Geological Survey projects (DD20243344 and DD20230700702), and the Special Fundamental Research Funds for China University of Geosciences (Beijing) (2-9-2024-093).

Institutional Review Board Statement: Not applicable.

Informed Consent Statement: Not applicable.

Data Availability Statement: The numerical data supporting this study are provided in the Supplementary Materials. Precise sampling coordinates are not publicly available due to project confidentiality requirements. Access may be requested from the corresponding author, subject to the applicable confidentiality requirements.

Acknowledgments: During the preparation of this manuscript, the authors used OpenAI Codex to assist with English language editing, manuscript revision and coding. The authors reviewed and verified the assisted content and take full responsibility for the final manuscript.

Conflicts of Interest: The authors declare no conflicts of interest.

References

1. Qin, H.-B.; Zhu, J.-M.; Zhu, Y.-X.; Lei, L. Speciation, sources, and fluxes of selenium in atmospheric environments. *Earth Environ.* **2009**, *37*, 304–314. (In Chinese) [CrossRef]
2. Wen, H.; Carignan, J. Reviews on atmospheric selenium: Emissions, speciation and fate. *Atmos. Environ.* **2007**, *41*, 7151–7165. [CrossRef]

3. Winkel, L.H.E.; Vriens, B.; Jones, G.D.; Schneider, L.S.; Pilon-Smits, E.; Bañuelos, G.S. Selenium Cycling Across Soil-Plant-Atmosphere Interfaces: A Critical Review. *Nutrients* **2015**, *7*, 4199–4239. [CrossRef] [PubMed]
4. Feinberg, A.; Maliki, M.; Stenke, A.; Sudret, B.; Peter, T.; Winkel, L.H.E. Mapping the drivers of uncertainty in atmospheric selenium deposition with global sensitivity analysis. *Atmos. Chem. Phys.* **2020**, *20*, 1363–1390. [CrossRef]
5. Feinberg, A.; Stenke, A.; Peter, T.; Winkel, L.H.E. Constraining Atmospheric Selenium Emissions Using Observations, Global Modeling, and Bayesian Inference. *Environ. Sci. Technol.* **2020**, *54*, 7146–7155. [CrossRef] [PubMed]
6. Feinberg, A.; Stenke, A.; Peter, T.; Hinckley, E.L.S.; Driscoll, C.T.; Winkel, L.H.E. Reductions in the deposition of sulfur and selenium to agricultural soils pose risk of future nutrient deficiencies. *Commun. Earth Environ.* **2021**, *2*, 101. [CrossRef]
7. Pan, Y.; Liu, J.; Zhang, L.; Cao, J.; Hu, J.; Tian, S.; Li, X.; Xu, W. Bulk Deposition and Source Apportionment of Atmospheric Heavy Metals and Metalloids in Agricultural Areas of Rural Beijing during 2016–2020. *Atmosphere* **2021**, *12*, 283. [CrossRef]
8. Breuninger, E.S.; Tolu, J.; Thurnherr, I.; Aemisegger, F.; Feinberg, A.; Bouchet, S.; Sonke, J.E.; Pont, V.; Wernli, H.; Winkel, L.H.E. Influences of sources and weather dynamics on atmospheric deposition of Se species and other trace elements. *Atmos. Chem. Phys.* **2024**, *24*, 2491–2510. [CrossRef]
9. Haugvaldstad, O.W.; Tang, H.; Kaakinen, A.; Bohm, K.; Groot Zwaaftink, C.D.; Grythe, H.; Stevens, T.; Zhang, Z.; Stordal, F. Spatial Source Contribution and Interannual Variation in Deposition of Dust Aerosols Over the Chinese Loess Plateau. *J. Geophys. Res. Atmos.* **2024**, *129*, e2023JD040470. [CrossRef]
10. Li, X.; Li, Y.; Li, Y.; Liu, M.; Huang, R.; Han, Z. Particle Size Control on Loess Geochemistry: Characteristics, Mechanisms, and Implications for Provenance Tracing. *Geochem. Geophys. Geosyst.* **2025**, *26*, e2024GC012046. [CrossRef]
11. Haygarth, P.M.; Jones, K.C.; Harrison, A.F. Selenium cycling through agricultural grasslands in the UK: Budgeting the role of the atmosphere. *Sci. Total Environ.* **1991**, *103*, 89–111. [CrossRef]
12. Hou, Q.; Yang, Z.; Ji, J.; Yu, T.; Chen, G.; Li, J.; Xia, X.; Zhang, M.; Yuan, X. Annual net input fluxes of heavy metals of the agro-ecosystem in the Yangtze River delta, China. *J. Geochem. Explor.* **2014**, *139*, 68–84. [CrossRef]
13. Yu, T.; Yang, Z.; Lv, Y.; Hou, Q.; Xia, X.; Feng, H.; Zhang, M.; Jin, L.; Kan, Z. The origin and geochemical cycle of soil selenium in a Se-rich area of China. *J. Geochem. Explor.* **2014**, *139*, 97–108. [CrossRef]
14. Song, T.; Cui, G.; Su, X.; He, J.; Tong, S.; Liu, Y. The origin of soil selenium in a typical agricultural area in Hamatong River Basin, Sanjiang Plain, China. *Catena* **2020**, *185*, 104355. [CrossRef]
15. Chen, X.; Yang, Z.-F.; Chen, Y.-L.; Yang, Q.; Wang, L.; Wei, X.-J. Selenium input flux in farmland soil of 9 counties in the middle east of Guangxi. *Geophys. Geochem. Explor.* **2020**, *44*, 820–829. (In Chinese) [CrossRef]
16. Eiche, E.; Nothstein, A.K.; Göttlicher, J.; Steininger, R.; Dhillon, K.S.; Neumann, T. The behaviour of irrigation induced Se in the groundwater-soil-plant system in Punjab, India. *Environ. Sci. Process. Impacts* **2019**, *21*, 957–969. [CrossRef] [PubMed]
17. De Feudis, M.; D'Amato, R.; Businelli, D.; Guiducci, M. Fate of selenium in soil: A case study in a maize (*Zea mays* L.) field under two irrigation regimes and fertilized with sodium selenite. *Sci. Total Environ.* **2019**, *659*, 131–139. [CrossRef] [PubMed]
18. Sun, G.X.; Meharg, A.A.; Li, G.; Chen, Z.; Yang, L.; Chen, S.C.; Zhu, Y.G. Distribution of soil selenium in China is potentially controlled by deposition and volatilization? *Sci. Rep.* **2016**, *6*, 20953. [CrossRef] [PubMed]
19. Li, X.; Hou, Q.; Duan, Y.; Li, Y.; Lin, K.; Li, B.; Sheng, W.; Wang, Y.; Su, R.; Gu, Z.; et al. Soil selenium enrichment in the Loess Plateau of China: Geogenic evidence, spatial distribution, and it's influence factors. *Chemosphere* **2023**, *340*, 139846. [CrossRef] [PubMed]
20. Zhou, W.-H.; Li, X.-Z.; Li, Y.-C.; Gao, Q.; Yang, Z.-F.; Duan, Y.-R. Geochemical characteristics of selenium in soils and crops and its significance in Yuanzhou District, Guyuan, Ningxia. *Geol. Rev.* **2023**, *69*, 795–808. (In Chinese) [CrossRef]
21. Blazina, T.; Sun, Y.; Voegelin, A.; Lenz, M.; Berg, M.; Winkel, L.H.E. Terrestrial selenium distribution in China is potentially linked to monsoonal climate. *Nat. Commun.* **2014**, *5*, 4717. [CrossRef] [PubMed]
22. Ministry of Land and Resources of the People's Republic of China. *Specifications for Geochemical Evaluation of Land Quality*; DZ/T 0295–2016; Geological Publishing House: Beijing, China, 2016. (In Chinese)
23. Yi, K.; Fan, W.; Chen, J.; Jiang, S.; Huang, S.; Peng, L.; Zeng, Q.; Luo, S. Annual input and output fluxes of heavy metals to paddy fields in four types of contaminated areas in Hunan Province, China. *Sci. Total Environ.* **2018**, *634*, 67–76. [CrossRef] [PubMed]
24. Department of Water Resources of the Ningxia Hui Autonomous Region. *Ningxia Water Resources Bulletin (2020)*; Department of Water Resources of the Ningxia Hui Autonomous Region: Yinchuan, China, 2021. (In Chinese)
25. Guyuan Water Conservancy Survey and Design Institute Co., Ltd. *Preliminary Design Report for the Guomiao Reservoir Rehabilitation Project in Yuanzhou District, Guyuan City*; Guyuan Water Conservancy Survey and Design Institute Co., Ltd.: Guyuan, China, 2023. (In Chinese)
26. Wang, Z.J. Some biogeochemical aspects of selenium in Chinese low-selenium belt. *Environ. Chem.* **1993**, *12*, 237–243. (In Chinese)
27. Li, R.; Yan, H.-F.; Zhang, L.; Miao, F.-F.; Mian, Y.-M.; Hou, X.-Q. Effects of Different Tillage Practices on Soil Physical Properties and Crop Yield in the Region of Southern Ningxia. *Sci. Agric. Sin.* **2023**, *56*, 3543–3555. [CrossRef]
28. Guyuan Municipal Natural Resources Bureau. *Guyuan Municipal Mineral Resources Master Plan (2021–2025)*; Guyuan Municipal Natural Resources Bureau: Guyuan, China, 2022. (In Chinese)

29. Sun, D.; Chen, F.; Bloemendal, J.; Su, R. Seasonal variability of modern dust over the Loess Plateau of China. *J. Geophys. Res. Atmos.* **2003**, *108*, 4665. [CrossRef]
30. Ma, T.; Huang, Y.; Deng, S.; Fu, B.; Luo, G.; Wang, J.; Hu, H.; Yuan, C.; Yao, H. The relationship between selenium retention and fine particles removal during coal combustion. *Fuel* **2020**, *265*, 116859. [CrossRef]
31. Xiao, L.; Ding, M.; Wei, C.; Zhu, R.; Zhao, R. The Impacts of Conservation Agriculture on Water Use and Crop Production on the Loess Plateau: From Know-What to Know-Why. *Sustainability* **2020**, *12*, 7449. [CrossRef]
32. He, J.; Hu, Y.; Shi, L.; Wang, H.; Tong, Y.; Dai, W.; Zhang, M. Spatio-Temporal Dynamics and Contributing Factors of Irrigation Water Use in the Loess Plateau. *Land* **2025**, *14*, 1286. [CrossRef]
33. Tolu, J.; Bouchet, S.; Helfenstein, J.; Hausheer, O.; Chékifi, S.; Frossard, E.; Tamburini, F.; Chadwick, O.A.; Winkel, L.H.E. Understanding soil selenium accumulation and bioavailability through size resolved and elemental characterization of soil extracts. *Nat. Commun.* **2022**, *13*, 6974. [CrossRef] [PubMed]

Disclaimer/Publisher's Note: The statements, opinions and data contained in all publications are solely those of the individual author(s) and contributor(s) and not of MDPI and/or the editor(s). MDPI and/or the editor(s) disclaim responsibility for any injury to people or property resulting from any ideas, methods, instructions or products referred to in the content.